Research Article Vol. 7, No. 3 / March 2019 / Photonics Research 311

PHOTONICS Research

Nearly lattice-matched molybdenum disulfide/gallium nitride heterostructure enabling high-performance phototransistors

Xinke Liu,[1,2] Yuxuan Chen,[1,2] Dabing Li,[1,2] Sheng-Wen Wang,[3] Chao-Cheng Ting,[3] Lin Chen,[4] Kah-Wee Ang,[5] Cheng-Wei Qiu,[5] Yu-Lun Chueh,[6] Xiaojuan Sun,[1,2,7] and Hao-Chung Kuo[3,8]

[1]State Key Laboratory of Luminescence and Applications, Changchun Institute of Optics, Fine Mechanics and Physics, Chinese Academy of Sciences, Changchun 130033, China
[2]Center of Materials Science and Optoelectronics Engineering, University of Chinese Academy of Sciences, Beijing 100049, China
[3]Department of Photonics and Institute of Electro-Optical Engineering, National Chiao Tung University, Hsinchu 300, Taiwan
[4]Department of Microelectronics, Fudan University, Shanghai 200433, China
[5]Department of Electrical and Computer Engineering, National University of Singapore, Singapore 117583, Singapore
[6]Department of Materials Science and Engineering, National Tsing Hua University, Hsinchu 300, Taiwan
[7]e-mail: sunxj@ciomp.ac.cn
[8]e-mail: hckuo@faculty.nctu.edu.tw

Received 11 January 2019; revised 16 January 2019; accepted 17 January 2019; posted 17 January 2019 (Doc. ID 357440); published 22 February 2019

Molybdenum disulfide (MoS_2)-based phototransistors are attractive for optical electronics in a large-scale size, such as transparent touch screens. However, most of the work done over the past decade has been on an opaque SiO_2/Si wafer with a small size (micrometer to millimeter). In this work, a large-scale multilayer MoS_2-based phototransistor has been fabricated on a transparent freestanding gallium nitride (GaN) wafer using a scalable chemical vapor deposition method. Due to the near lattice match and small thermal expansion mismatch between GaN and MoS_2, the as-grown multilayer MoS_2-on-GaN film shows high material quality in terms of low full width at half-maximum (~5.16 cm^{-1}) for the E^1_{2g} Raman mode and a high absorption coefficient (~10^6 cm^{-1}) in the wavelength range of 405–638 nm. Under a wavelength of 405 nm at an incident power of 2 mW and applied voltage of 9 V, the fabricated MoS_2-on-GaN phototransistor achieved a maximum responsivity of 17.2 A/W, a photocurrent gain of 53.6, and an external quantum efficiency of 5289%, with specific detectivity (~10^{10}–10^{12} Jones) and low noise equivalent power (10^{-12}–10^{-14} $W/Hz^{1/2}$) in the visible range of 405–638 nm. A typical response time of 0.1–4 s in the ambient air has also been recorded for the demonstrated MoS_2-on-GaN phototransistor. Our work paves a technologic stepping stone for MoS_2-based phototransistors for multifunctional transparent and touch-based optoelectronics in the future.

https://doi.org/10.1364/PRJ.7.000311

1. INTRODUCTION

Molybdenum disulfide (MoS_2), as a typical example of the two-dimensional material family, is a layered transition-metal dichalcogenide semiconductor that has no surface dangling bonds and high thermal stability (~1100°C). Due to its high carrier mobility, reasonable bandgap, and high light absorbance, MoS_2 has attracted intense research interest because of its potential applications in nanoelectronics, including touch-sensor panels, image sensors, solar cells, and communication devices [1–11]. As compared with graphene (zero bandgap), multilayer (ML) MoS_2 is an indirect semiconductor with a bandgap energy of 1.2 eV, while single-layer (1L) MoS_2 is a direct semiconductor (1.8 eV). MoS_2-based electronic devices with a high current on/off ratio (10^6–10^8), mobility up to ~140–200 $cm^2 \cdot V^{-1} \cdot s^{-1}$, and low subthreshold swing (~70–80 mV/decade) have been reported in the literature [12–14]. On the other hand, the MoS_2-based phototransistors have also achieved significant progress since the first demonstration of exfoliated monolayer MoS_2 phototransistors with a responsivity of ~7.5 mA/W at a wavelength of 750 nm [15]. The responsivity of ~880 A/W has also been demonstrated on the exfoliated monolayer MoS_2 phototransistor in the depletion operation region [1]. The response time or the rise time is on the order of a few seconds, which can be further reduced to microseconds with the help of a gate pulse to reset the conductivity of the device channel, since the trap state plays an important role in the photocurrent

generation mechanism. Given the large surface-to-volume ratio, the absorbates play a major role in the properties of layered MoS_2 material, and changed absorbates also reduce the photoresponse as they suppress the lifetime of trapped carriers by acting as recombination centers. Higher responsivity of ~2200 A/W is obtained for the monolayer MoS_2 phototransistor in the vacuum condition [16]. Most of these devices were based on small size MoS_2 microsheets fabricated by mechanical exfoliation from bulk crystals or chemical vapor deposition (CVD) synthesis. Nevertheless, the applications were restricted by the limited capability in producing high-quality and uniform large-area MoS_2 film. To integrate MoS_2 into scalable manufacturing, a large-scale synthesis method to fabricate high-quality MoS_2 film with precise control of thickness is essential. Bottom-up methods such as CVD [17], thermal evaporation [18,19], magnetron sputtering [20], electrochemical lithiation processes [21,22], and sulfurization of molybdenum oxides [23] have been introduced for fabricating large-scale layered MoS_2 on a SiO_2/Si substrate. The reported mobility obtained from the exfoliated monolayer MoS_2 shows a significant degradation in the range of 0.1–10 $cm^2 \cdot V^{-1} \cdot s^{-1}$ [24,25]. The field effect mobility at room temperature of MoS_2 is limited by phonon scattering in the range of 200–500 $cm^2 \cdot V^{-1} \cdot s^{-1}$ [26]. Charge traps (up to $\sim 10^{15}$ cm^{-2}) located at the interface between the MoS_2 and SiO_2 layer, and also charged impurity scattering within the SiO_2 layer, have been identified as the main causes for low mobility in MoS_2 electronic devices at room temperature [10,27,28]. In order to eliminate the effect due to the underlying SiO_2 layer, such as charge scattering, it is proposed in this work that the MoS_2 film is grown on nearly lattice-matched (0.8%) freestanding (FS) gallium nitride (GaN), which has a wide energy bandgap (3.4 eV) and is highly chemically stable and transparent. Recently, MoS_2-based photodetectors on sapphire have been demonstrated, but the devices show a low responsivity (less than 1 A/W), which is due to the challenge of growing high-quality MoS_2 film on the large lattice mismatch (~50%) and the large thermal expansion coefficient (TEC) mismatch sapphire substrate (lattice $a \sim 0.4758$ nm; TEC $\sim 7.5 \times 10^{-6}$ K^{-1}) [29,30]. A bulk GaN wafer was used to ensure that the GaN wafer has zero local strain, and its defect density is below $\sim 10^4$–10^5 cm^{-2}, which is much lower as compared to the defect density of the SiO_2 layer [31,32]. As compared with monolayer MoS_2, ML MoS_2 film is attractive for phototransistor application, which is not only due to its smaller bandgap, extended detection range, and larger absorption, but also the easier growth in a large-scale uniform film. However, the responsivity of the ML MoS_2 phototransistor without any boost technique is lower, which could be due to its indirect bandgap.

In order to achieve better quality, as-grown MoS_2 film, large-scale ML MoS_2 film, has been grown on the nearly perfect lattice-matched and transparent FS GaN wafer in this work. MoS_2-on-GaN phototransistors have been fabricated in a typical semiconductor fabrication process and fully characterized. Detailed material studies using Raman spectroscopy, X-ray photoelectron spectroscopy (XPS), transmission electron microscopy (TEM), and absorption techniques have been carried out. Maximum responsivity R of 17.2 A/W, highest specific detectivity D of $\sim 1.8 \times 10^{12}$ Jones, and the lowest noise equivalent power (NEP) of $\sim 9.6 \times 10^{-14}$ $W/Hz^{1/2}$ have been achieved for the fabricated MoS_2-on-GaN phototransistors with a typical response time of 0.1–4 s in the visible wavelength range under ambient air.

2. METHOD

A. Sample Preparation and Device Fabrication

Two-inch FS GaN substrate (350 μm thick) with (0001) orientation was grown by hydride vapor phase epitaxy (HVPE). HCl/metal Ga, ammonia, and a N_2/H_2 mixture were used as the Ga source, nitrogen source, and carrier gas, respectively. The growth rate was typically about 150 μm/h. After HVPE growth, the Ga surface was further polished by chemical mechanical polishing (CMP). The FS GaN substrate went through a precleaning process, which consisted of a 5-min acetone, a 5-min isopropanol degreasing step, and a 2-h piranha solution (H_2O_2:H_2SO_4 = 1:3) immersion step for the organic residue removal. 0.08 mg of MoO_3 was spread uniformly over 2–3 cm in an alumina crucible and FS GaN wafer growth substrate was placed upside down on the crucible. Sulfur powder (1 g) was placed upstream in 30 sccm of argon gas flow. Few layer FS MoS_2 was grown at 800°C for 5 min. Ti(5 nm)/Al(50 nm) was directly deposited as an electrode using a shallow mask without a film transfer process. Due to the limitation of the CVD chamber diameter, 50 mm FS-GaN was cut into small pieces for CVD growth (1 cm by 1 cm).

B. Materials and Electrical Characterizations

Raman spectra were collected in a Renishaw inVia confocal system in the backscattering configuration. The wavelength of the laser was 514.5 nm (2.41 eV) from an argon ion laser; a grating of 2400 grooves $\cdot$ mm^{-1} was used to obtain more details of the line shapes of the Raman band. The laser power on the sample was set at around 1.0 μW to avoid laser-induced heating. The Si peak at 520 cm^{-1} was used as a reference for wavelength calibration. The absorbance spectra were measured with a SHIMADZU-2450 UV-visible spectrometer in the spectral range of 380–900 nm. XPS profiles were obtained using a VG ESCALAB 220i-XL system with a monochromatized Al Kα (1486.6 eV) X-ray source (a constant pass energy of 20 eV). A Keithley 4200-SCS semiconductor analyzer was used to measure the *I-V* characteristics and responsivity of the MoS_2-on-GaN phototransistor.

3. RESULTS AND DISCUSSION

Figure 1(a) schematically illustrates the experimental CVD setup used in this work. An FS undoped GaN wafer was used as the starting substrate for the one-step direct growth of ML MoS_2 film, in which MoO_3 and sulfur powder were used as precursors. The detailed growth process can be found in the previous published work [33]. Due to the limitation of the furnace diameter, the size of the FS GaN wafer is 1 cm by 1 cm. The as-grown MoS_2-on-GaN sample was characterized using Raman measurement. As shown in Fig. 1(b), Raman spectra from the four locations indicated by the arrows shown in the inset are shown. The A_{1g} mode related to the out-of-plane vibration of sulfur atoms and the E^1_{2g} mode associated with the

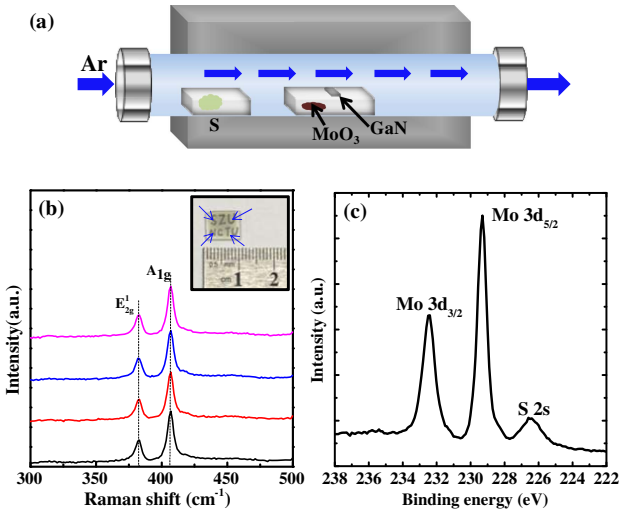

Fig. 1. (a) Illustration of the experimental setup of CVD in this work. The Ga face of the FS GaN wafer is faced down, and ML MoS_2 is grown on the Ga surface. The growth temperature and duration time were 800°C and 5 min, respectively. (b) Raman spectra of the as-grown MoS-on-GaN sample from the four locations indicated by the arrows shown in the inset, and the letters SZU and NCTU being an abbreviation of "Shenzhen University" and "National Chiao Tung University" are clearly seen. (c) Core-level XPS spectrum of Mo 3d and S 2s of the as-grown MoS-on-GaN sample.

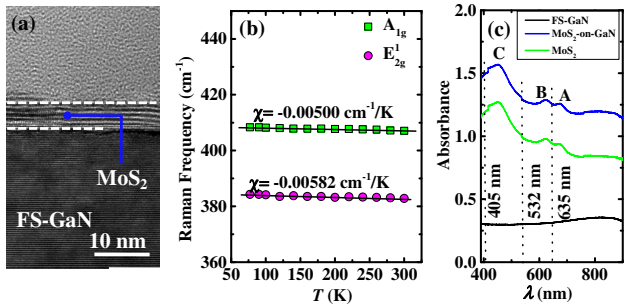

Fig. 2. (a) Cross-sectional TEM image of the as-grown MoS_2-on-GaN sample. The measured MoS_2 film thickness is ~5 nm, and the number of MoS_2 layers is ~5 layers. (b) Effect of temperature variation on the Raman modes of A_{1g} and E^1_{2g} modes of MoS_2-on-GaN film; (c) absorbance of FS GaN, as-grown MoS_2-on-GaN film, and the MoS_2 layer as a function of incident wavelength. The absorbance of MoS_2 could be obtained by subtracting the absorbance value of FS GaN from that of the as-grown MoS_2-on-GaN sample.

in-plane vibration of Mo and sulfur atoms, can be clearly observed in Fig. 1(b). The MoS_2 crystalline quality can be reflected by the full width at half-maximum (FWHM) of the E^1_{2g} Raman peak. The value of FWHM for the E^1_{2g} Raman peak in this work is about ~5.16 cm^{-1}, which is larger than 3.7 cm^{-1} of the exfoliated MoS_2 film, but smaller than 6.5 cm^{-1} of as-grown MoS_2 film by CVD [33]. This could be related with certain crystalline imperfections, for example, sulfur vacancies and crystalline grain boundary in the synthesized thin film. The lower FWHM value of the E^1_{2g} for as-grown MoS_2-on-GaN film does indicate the advantage by the lattice-matched MoS_2-on-GaN technique. The thickness of MoS_2 film can be estimated by the frequency difference (Δk) between the E^1_{2g} and A_{1g} Raman peaks. As shown in Fig. 1(b), the Δk value of the synthesized MoS_2-on-GaN film is about 24.97 cm^{-1}, which corresponds to more than 5–6 layers. According to the Raman peak position for the different locations, the uniformity of as-grown MoS_2-on-GaN is excellent, since the Raman peak position has little shift for the different locations. XPS measurement was employed to determine the composition of MoS_2 film. Figure 1(c) shows the core-level XPS spectrum of Mo 3d and S 2s. The peak binding energy for Mo $3d_{3/2}$, Mo $3d_{3/2}$, and S 2s is 232.45, 229.32, and 226.45 eV, respectively, which is consistent with reported values in the literature. Also, the peak (~235.6 eV) related to Mo-O bonding is absent here, indicating MoO_x overdeposition does not occur here. The S: Mo atomic ratio is estimated to be 2.03, which is close to the stoichiometric MoS_2, and the S 2s peak is located at 226.45 eV, which is the characteristic of the stoichiometric MoS_2 [34,35].

Figure 2(a) shows the cross-sectional TEM image of the as-grown MoS_2-on-GaN sample. The measured MoS_2 film thickness is ~5 nm, and the number of MoS_2 layers is ~5, which is consistent with the Raman frequency difference (Δk). Figure 2(b) shows the effect of temperature variation on the Raman modes of the A_{1g} and E^1_{2g} modes of MoS_2-on-GaN film. Temperature-dependent Raman studies of the as-grown MoS_2-on-GaN film and as-grown MoS_2-on-SiO_2 film under the same growth condition in the range of 77–300 K under a 514 nm excitation laser were carried out. The peak positions for A_{1g} and E^1_{2g} modes versus temperature were fitted using the Grüneisen model: $\omega(T) = \omega_0 + xT$, where ω_0 is the Raman peak position at 0 K, x is the first-order temperature coefficient, and T is the temperature. The slope of fitted lines gives the first-order temperature coefficient, as shown in Fig. 2(b). The first-order temperature coefficients x of the A_{1g} and E^1_{2g} modes of as-grown MoS_2-on-GaN film are −0.00500 cm^{-1}/K and −0.00582 cm^{-1}/K, respectively. Similarly, the first-order temperature coefficients x of the A_{1g} and E^1_{2g} modes of as-grown MoS_2-on-SiO_2 film were also measured to be −0.00520 cm^{-1}/K and −0.00490 cm^{-1}/K, respectively. The first-order temperature coefficient x of the A_{1g} mode related to out-of-plane vibration of sulfur atoms has little difference between as-grown MoS_2-on-GaN film and as-grown MoS_2-on-SiO_2 film. However, the first-order temperature coefficient x of the E^1_{2g} mode for as-grown MoS_2-on-GaN film is ~19% higher than that of as-grown MoS_2-on-SiO_2 film. The E^1_{2g} Raman mode of MoS_2 is a stress-sensitive in-plane vibration mode. Due to the large TEC mismatch between MoS_2 (1.2×10^{-5} K^{-1}) and SiO_2 (5.5×10^{-7} K^{-1}), tensile strain within the as-grown MoS_2 film on SiO_2 is acquired during the cool-down step of CVD growth. As compared with MoS_2-on-SiO_2 film, the TEC mismatch between MoS_2 (1.2×10^{-5} K^{-1}) and GaN (3.2×10^{-6} K^{-1}) is smaller, or tensile strain within the MoS_2-on-GaN film is smaller [36]. Due to the smaller tensile strain within the MoS_2-on-GaN film, the first-order temperature coefficient x of the E^1_{2g} mode is slightly higher than that of MoS_2-on-SiO_2 film, since the thermal stability can be enhanced by additional stress [36]. Figure 2(c) shows the absorbance of FS GaN and as-grown MoS_2-on-GaN as a function

of incident wavelength. Based on the measured absorbance values of FS GaN and as-grown MoS_2-on-GaN, the absorbance value of MoS_2 film could be calculated by subtracting the absorbance value of FS GaN from that of as-grown MoS_2-on-GaN, and plotted as a function of incident wavelength in Fig. 2(c). Two excitonic peaks (A and B) located at 672.40 nm and 622.61 nm, respectively, are observed for MoS_2 film, and this arises from the K point of the Brillouin zone. The energy difference between exciton A and exciton B is due to the spin-orbital splitting in the valence band of MoS_2. In addition to band-edge associated excitons, exciton C located at 450.82 nm is also observed in Fig. 2(c), which is due to the band-nesting effect and further results in a strong optical absorption even for excitation energy far beyond the bandgap value. Based on the Beer–Lambert law, $I_t = I_0 e^{-\alpha t}$, where I_t is the intensity of transmitted light, I_0 is the intensity of original light, α is the absorption coefficient, and t is the MoS_2 thickness. The "absorbance A" is defined as $A = \log_{10}(I_0/I_t)$. For example, 90% of light is absorbed when the value of absorbance A is 1. As shown in Fig. 2(c), the values of absorbance A of the MoS_2 film are 1.19, 1.02, and 0.96, for wavelengths of 405, 532, and 638 nm, respectively, indicating 94%, 90%, and 89% of incident light intensity is absorbed at that specific wavelength. Lasers with these three different wavelengths (405, 532, and 638 nm) are chosen for phototransistor study later. By decreasing the wavelength from 638 to 405 nm, the absorption rate is increased for MoS_2 film grown on GaN. The absorption coefficient α can be calculated using the equation: $\alpha = \ln(10)A/t$. Therefore, the calculated values of absorption coefficient α are 5.45×10^6 cm^{-1}, 4.70×10^6 cm^{-1}, and 4.42×10^6 cm^{-1}, at wavelengths of 405, 532, and 638 nm, respectively [37]. The obtained value of absorption coefficient α for MoS_2-on-GaN film is about 1 order of magnitude higher than that reported for MoS_2-on-SiO_2 film, which could lead to a highly responsive MoS_2 phototransistor. The high absorption coefficient α for MoS_2-on-GaN film could be due to the high-quality MoS_2 film grown on the nearly lattice-matched and smaller thermal expansion mismatch FS GaN substrate.

Figure 3(a) shows the fabricated MoS_2 phototransistors on a transparent FS GaN sample with a size of 1 cm by 1 cm, in which a device array has been fabricated. With the method proposed in this work, it can be used for fabricating MoS_2 phototransistors on a large scale. Figure 3(b) shows the 3D schematic view of the MoS_2-on-GaN phototransistor on the transparent FS GaN wafer, and the device footprint size is ~0.01 cm^2, with an active area of 0.0008 cm^{-2}. As shown in Fig. 3(c), the current ratio of light/dark for the fabricated MoS_2-on-GaN phototransistors is ~10^1–10^2 at applied voltage of 10 V and incident power of 10 mW, with a laser spot diameter of 2 mm. It is noted that the photocurrent under a 405 nm laser illumination is about ~3–4 times higher than that under a 638 nm laser illumination, which is due to both the high absorption ratio and photocurrent gain mechanism. Photocurrent I_{ph} under different incident powers of the MoS_2-on-GaN phototransistor was measured under three laser wavelengths of 638, 532, and 638 nm, respectively. The photocurrent generated from the MoS_2-on-GaN phototransistor is solely determined by the incident power at a constant voltage. The photogating

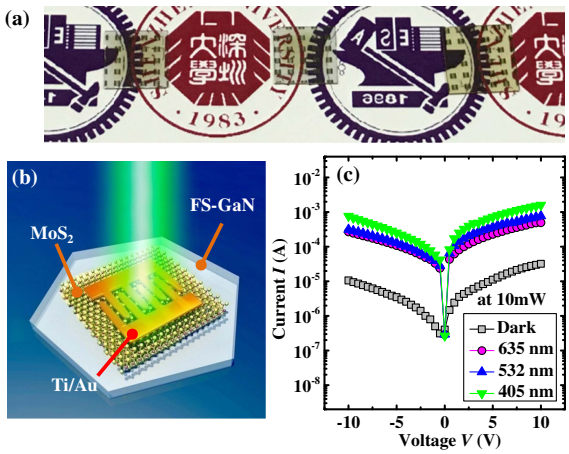

Fig. 3. (a) Photo image of the fabricated transparent ML MoS_2-on-GaN phototransistors; (b) 3D schematic view of the MoS_2-on-GaN phototransistor on a transparent FS GaN wafer; (c) the current ratio of light/dark for the fabricated MoS_2-on-GaN phototransistors is ~10^1–10^2 at an applied voltage of 10 V and incident power of 10 mW with a laser spot diameter of 2 mm.

effect, due to the trapped electrons/holes underneath the channel, is not observed for MoS_2-on-GaN phototransistors, which is due to the high quality and large bandgap of GaN, as compared with the case of MoS_2-based photodetectors using a SiO_2/Si wafer. To quantify the photosensitivity of the fabricated phototransistor, the photoresponsivity R is calculated by the expression: $R = I_{ph}$/(power density × active area), where the photocurrent I_{ph} is defined as $I_{ph} = I_{light} - I_{dark}$. As shown in Figs. 4(a)–4(c), photoresponsivity R under three laser wavelengths of 638, 532, and 405 nm, respectively, is plotted as a function of incident laser power. It is observed that the photoresponsivity R is slightly increased as the incident laser power decreases, which is also reported in MoS_2 and other 2D material (black phosphorus, BP)-based phototransistors [1,15,38].

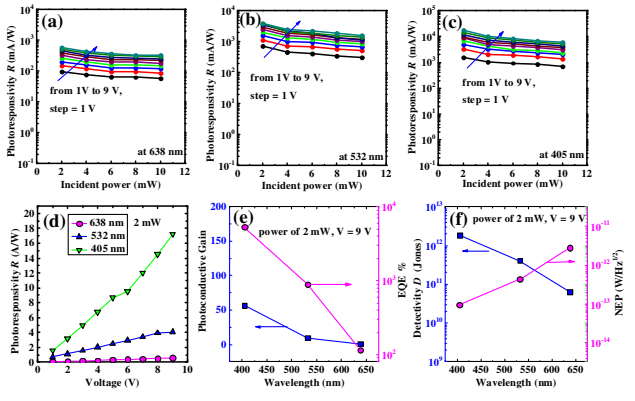

Fig. 4. Photoresponsivity R under three laser wavelengths of (a) 638, (b) 532, and (c) 405 nm plotted as a function of incident laser power. (d) Photoresponsivity R as a function of applied voltage for three laser wavelengths (638, 532, and 405 nm) at a laser power of 2 mW; (e) photoconductive gain G and EQE as a function of the incident wavelength with an applied voltage of 9 V and power of 2 mW; (f) specific detectivity D and NEP as a function of the incident wavelength with an applied voltage of 9 V and power of 2 mW.

This could be due to less frequent carrier recombination and longer carrier lifetime under a weaker illumination. Figure 4(d) shows photoresponsivity R as a function of applied voltage for three laser wavelengths at a laser power of 2 mW. At 2 mW laser illumination power, a peak photoresponsivity R of 0.59, 2.78, and 17.2 A/W is obtained for a laser wavelength of 638, 532, and 405 nm, respectively. By increasing the voltage, the photoresponsivity R is linearly increased in Fig. 4(d). Under a higher applied voltage, the electrical field across the active region is increased, which increases the drift velocity of photogenerated electron-hole carriers or increases the photogenerated current, leading to a larger photoresponsivity R. Also, it is noted that a larger photoresponsivity R is obtained at a shorter wavelength (405 nm), as compared with the other two wavelengths (638 and 532 nm); this is due to the higher light absorption at 405 nm, as shown in Fig. 2(c). This wavelength-dependent photoresponsivity corresponds well with the fact that higher excitation energy enhances the conversion of photoelecronics.

To further evaluate the performance of the MoS_2-on-GaN phototransistor, photoconductive gain G and external quantum efficiency (EQE) are also calculated and shown in Fig. 4(e). Photoconductive gain G, indicating how many carriers of the photocurrent can be generated by one absorbed photon, can be estimated by the equation $G = (I_{ph}/P_{abs})(h\nu/q)$, where P_{abs} is the power absorbed, h is Planck's constant, ν is the frequency of the incident laser, and q is the elementary charge. The value of P_{abs} equals μP_{in}, where μ is the absorption percentage and P_{in} is the incident power. The absorption percentage at a specific wavelength has been discussed in Fig. 2(c). As the laser wavelength decreases from 638 to 405 nm, the photoconductive gain G is increased from 1.3 to 56.3, indicating that a larger number of photogenerated electron-hole carriers are populated. EQE, defined as the number of photogenerated carriers collected per incident photon, can be calculated by the equation $EQE = R \times (h\nu/q)$. As shown in Fig. 4(e), EQE increased from 115% to 5289%, as the laser wavelength decreased from 638 to 405 nm. The maximum photoresponsivity R of 17.2 A/W, the maximum photoconductive gain G of 56.3, and the maximum EQE of 5289% are obtained under a 405 nm laser illumination at an applied voltage of 9 V and power of 2 mW, which is better than the reported values for MoS_2 and other 2D material (BP)-based phototransistors [38].

To evaluate the detection limit of our device and assume the short noise from the dark current is the major contributor to the total noise, the specific detectivity D is calculated by the equation $D = A^{1/2}/NEP$, where A is the device active area, and NEP is the noise equivalent power and defined as the excitation power needed to generate a signal equal to the noise level in the 1 Hz bandwidth. NEP can be estimated by the equation $NEP = (2qI_{dark}\Delta f)^{1/2}/R$, where I_{dark} is the dark current, Δf is the bandwidth, and R is the photoresponsivity. With the measured wavelength range of 405–638 nm, the specific detectivity D is $\sim 6.3 \times 10^{10}$–1.8×10^{12} Jones, and the NEP is $\sim 2.8 \times 10^{-12}$–9.6×10^{-14} W/Hz$^{1/2}$, as shown in Fig. 4(f). The low NEP of the MoS_2-on-GaN phototransistor has the potential to detect subpicowatt illumination power with half-a-second integration time. Although the performance of the MoS_2-on-GaN phototransistor in this work shows much inferior performance to a silicon photodiode (R of ~300 A/W and D of $\sim 10^{13}$ Jones) [37], their performance is better than phototransistors based on graphene (R of ~1–6.1 mA/W) or single layer MoS_2 (R of 7.5 mA/W). In addition, the MoS_2-on-GaN phototransistor in this work consists of a simple n-type channel, which is easier to fabricate than a Si p-n photodiode. Future work involving optimization of the device architecture and processing will greatly enhance the performance of MoS_2-on-GaN phototransistors.

Photoswitching characteristics have also been investigated under the three different laser illuminations (638, 532, and 405 nm) for various incident powers at a fixed voltage of 3 V. The stability of the switching behavior is demonstrated by applying multiple illuminations on the device for 10 s. Figure 5(a) shows the photocurrent as a function of time under the alternative dark and illumination conditions at different laser wavelengths with a fixed incident power of 6 mW and a fixed voltage of 3 V. Under illumination, the current rises to a high value (on-state) and then returns to a low value (off-state) when the light is off. The rise and fall times are taken from 10% to 90% of the maximum photocurrent and from 90% to 10% of the maximum photocurrent, respectively, as shown in Fig. 5(b). Figures 5(c) and 5(d) show the rise time t_{rise} and fall time t_{fall} as functions of the incident power for three different laser illuminations (638, 532, and 405 nm) with a fixed voltage of 3 V. The rise time t_{rise} shows wavelength-dependent behavior, but is less sensitive to the incident power. As the illumination laser wavelength decreases from 638 to 405 nm, the average rise time t_{rise} decreases from 4.2 s to

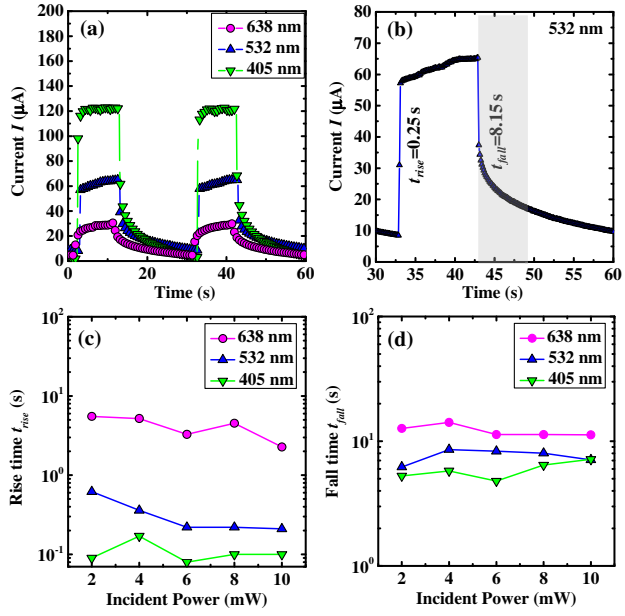

Fig. 5. (a) Photocurrent as a function of time under the alternative dark and illumination conditions at different laser wavelengths (638, 532, and 405 nm) with a fixed incident power of 6 mW and a fixed voltage of 3 V; (b) the rise and fall times are taken from 10% to 90% of the maximum photocurrent and from 90% to 10% of the maximum photocurrent, respectively. (c) Rise time t_{rise} and (d) fall time t_{fall} as a function of incident power for three different laser illuminations (638, 532, and 405 nm) with a fixed voltage of 3 V.

0.1 s. The value of rise time t_{rise} depends on a charging or trapping process under the laser illumination. The rise time t_{rise} obtained here is still lower as compared with that of graphene (tens of picoseconds), as the carrier transport in graphene is ballistic and very fast [39–41], but is comparable to the reported monolayer MoS_2-based phototransistors [1]. The field effective mobility is extracted from the fabricated MoS_2 field effect transistor, and the average value of the field effective mobility is about 3.5 $cm^2 \cdot V^{-1} \cdot s^{-1}$. By further enhancing the carrier mobility of MoS_2, such as oxide passivation, the rise time t_{rise} here can be further reduced. As discussed in Fig. 2(c), it is noted that the absorption rate is higher under a 405 nm laser illumination, leading to generating more electron-hole carriers at a given time and filling up traps within the channel in a shorter duration. This explains that the MoS_2-on-GaN phototransistor shows a shorter rise time for shorter laser wavelengths. When the laser is switched off, the photocurrent does not decrease to the dark level immediately, but exponentially decreases. The observation of a persistent photocurrent is due to the trapped long-range Coulomb potentials, which could be from the charged impurities at the MoS_2/GaN interface or within MoS_2, thus drastically affecting the recombination of electron-hole pairs. The photocurrent during the fall time can be fitted using the equation $I_{ph} = I_{dark} + B \exp(t/\tau)$, where B is a scaling constant, t is the time, and τ is the time constant of the traps or relaxation time constant. The fitted relaxation time constant of the three laser wavelength cases is almost identical (~9.13 s), which explains that the fall time t_{fall} is less sensitive to the laser wavelength, since the fall time is dominated by the decharging or detrapping process, which is only related to the traps within the MoS_2-on-GaN sample. The MoS_2-on-GaN phototransistor in this work shows a typical rise time t_{rise} of 0.1–4 s and fall time t_{fall} of 9 s, which is similar to the corresponding value observed in the mechanical exfoliated monolayer MoS_2 phototransistor and graphene-quantum dot values [41]. It is believed that the surrounding of the MoS_2 plays an important role in photocurrent switching behavior, with different surface treatment able to reduce the fall time in the 0.3–4000 s range, due to the differences in surface hydrophobicity [42,43]. The photocurrent switching performance of the MoS_2-on-GaN phototransistor can be further improved by proper device passivation or an encapsulating technique.

4. CONCLUSION

Using the one-step CVD growth method, high-quality and large-scale ML MoS_2 film has been grown on a transparent nearly lattice-matched FS GaN wafer, which can be called transparent "MoS_2-on-GaN" technology. The fabricated MoS_2-on-GaN phototransistor shows high responsivity of 17.2 A/W at a laser wavelength of 405 nm, due to the high absorption coefficient of MoS_2-on-GaN film. In addition, high photocurrent gain, high EQE, high specific detectivity, and low NEP have been achieved for a transparent ML MoS_2-on-GaN phototransistor in the visible range (405, 532, and 638 nm), and it shows robust on/off photocurrent switching with a typical response time of 0.1–4 s. Transparent "MoS_2-on-GaN" technology developed in this work can be attractive for a variety of industry transparent applications, including touch-sensor panels, image sensors, and communication devices.

Funding. National Science Fund for Distinguished Young Scholars (61725403); National Key Research and Development Plan (2017YFB0403000); National Natural Science Foundation of China (NSFC) (61504083, 61634005).

Acknowledgment. We thank the State Key Laboratory of Luminescence and Applications for the use of their equipment.

REFERENCES

1. O. Lopez-Sanchez, D. Lembke, M. Kayci, A. Radenovic, and A. Kis, "Ultrasensitive photodetectors based on monolayer MoS_2," Nat. Nanotechnol. **8**, 497–501 (2013).
2. X. Liu, T. Galfsky, Z. Sun, F. Xia, E.-C. Lin, Y.-H. Lee, S. Kéna-Cohen, and V. M. Menon, "Strong light-matter coupling in two-dimensional atomic crystals," Nat. Photonics **9**, 30–34 (2015).
3. X. Liu, J. Wu, W. Yu, L. Chen, Z. Huang, H. Jiang, J. He, Q. Liu, Y. Lu, D. Zhu, W. Liu, P. Cao, S. Han, X. Xiong, W. Xu, J.-P. Ao, K.-W. Ang, and Z. He, "Monolayer $W_xMo_{1-x}S_2$ grown by atmospheric pressure chemical vapor deposition: bandgap engineering and field effect transistors," Adv. Funct. Mater. **27**, 1606469 (2017).
4. Q. H. Wang, K. Kalantar-Zadeh, A. Kis, J. N. Coleman, and M. S. Strano, "Electronics and optoelectronics of two-dimensional transition metal dichalcogenides," Nat. Nanotechnol. **7**, 699–712 (2012).
5. W. C. Tan, Y. Cai, R. J. Ng, L. Huang, X. Feng, G. Zhang, Y. W. Zhang, C. A. Nijhuis, X. Liu, and K. W. Ang, "Few-layer black phosphorus carbide field-effect transistor via carbon doping," Adv. Mater. **29**, 1700503 (2017).
6. Y. Liu, Y. Cai, G. Zhang, Y.-W. Zhang, and K.-W. Ang, "Al-doped black phosphorus p-n homojunction diode for high performance photovoltaic," Adv. Funct. Mater. **27**, 1604638 (2017).
7. F. H. Koppens, T. Mueller, P. Avouris, A. C. Ferrari, M. S. Vitiello, and M. Polini, "Photodetectors based on graphene, other two-dimensional materials and hybrid systems," Nat. Nanotechnol. **9**, 780–793 (2014).
8. K. F. Mak and J. Shan, "Photonics and optoelectronics of 2D semiconductor transition metal dichalcogenides," Nat. Photonics **10**, 216–226 (2016).
9. L. Britnell, R. M. Ribeiro, A. Eckmann, R. Jalil, B. D. Belle, A. Mishchenko, Y. J. Kim, R. V. Gorbachev, T. Georgiou, S. V. Morozov, A. N. Grigorenko, A. K. Geim, C. Casiraghi, A. H. Castro Neto, and K. S. Novoselov, "Strong light-matter interactions in heterostructures of atomically thin films," Science **340**, 1311–1314 (2013).
10. Y. Xue, Y. Zhang, Y. Liu, H. Liu, J. Song, J. Sophia, J. Liu, Z. Xu, Q. Xu, Z. Wang, J. Zheng, Y. Liu, S. Li, and Q. Bao, "Scalable production of a few-layer MoS_2/WS_2 vertical heterojunction array and its application for photodetectors," ACS Nano **10**, 573–580 (2016).
11. Z.-Q. Xu, Y. Zhang, S. Lin, C. Zheng, Y. L. Zhong, X. Xia, Z. Li, P. J. Sophia, M. S. Fuhrer, Y.-B. Cheng, and Q. Bao, "Synthesis and transfer of large-area monolayer WS_2 crystals: moving toward the recyclable use of sapphire substrates," ACS Nano **9**, 6178–6187 (2015).
12. S. Das, H.-Y. Chen, A. V. Penumatcha, and J. Appenzeller, "High performance multilayer MoS_2 transistors with scandium contacts," Nano Lett. **13**, 100–105 (2013).
13. D. Ovchinnikov, A. Allain, Y.-S. Huang, D. Dumcenco, and A. Kis, "Electrical transport properties of single-layer WS_2," ACS Nano **8**, 8174–8181 (2014).
14. X. Liu, J. Hu, C. Yue, N. Della Fera, Y. Ling, Z. Mao, and J. Wei, "High performance field-effect transistor based on multilayer tungsten disulfide," ACS Nano **8**, 10396–10402 (2014).
15. Z. Yin, H. Li, H. Li, L. Jiang, Y. Shi, Y. Sun, G. Lu, Q. Zhang, X. Chen, and H. Zhang, "Single-layer MoS_2 phototransistors," ACS Nano **6**, 74–80 (2012).

16. W. Zhang, J. K. Huang, C. H. Chen, Y. H. Chang, Y. J. Cheng, and L. J. Li, "High-gain phototransistors based on a CVD MoS_2 monolayer," Adv. Mater. **25**, 3456–3461 (2013).
17. Y. H. Lee, X. Q. Zhang, W. Zhang, M. T. Chang, C. T. Lin, K. D. Chang, Y. C. Yu, J. T. Wang, C. S. Chang, L. J. Li, and T. W. Lin, "Synthesis of large-area MoS_2 atomic layers with chemical vapor deposition," Adv. Mater. **24**, 2320–2325 (2012).
18. K.-K. Liu, W. Zhang, Y.-H. Lee, Y.-C. Lin, M.-T. Chang, C.-Y. Su, C.-S. Chang, H. Li, Y. Shi, H. Zhang, C.-S. Lai, and L.-J. Li, "Growth of large-area and highly crystalline MoS_2 thin layers on insulating substrates," Nano Lett. **12**, 1538–1544 (2012).
19. Y. Zhan, Z. Liu, S. Najmaei, P. M. Ajayan, and J. Lou, "Large-area vapor-phase growth and characterization of MoS_2 atomic layers on a SiO_2 substrate," Small **8**, 966–971 (2012).
20. Q. Feng, Y. Zhu, J. Hong, M. Zhang, W. Duan, N. Mao, J. Wu, H. Xu, F. Dong, F. Lin, C. Jin, C. Wang, J. Zhang, and L. Xie, "Growth of large-area 2D $MoS_{2(1-x)}Se_{2x}$ semiconductor alloys," Adv. Mater. **26**, 2648–2653 (2014).
21. Y. Peng, Z. Meng, C. Zhong, J. Lu, W. Yu, Y. Jia, and Y. Qian, "Hydrothermal synthesis and characterization of single-molecular-layer MoS_2 and $MoSe_2$," Chem. Lett. **30**, 772–773 (2001).
22. G. Eda, H. Yamaguchi, D. Voiry, T. Fujita, M. Chen, and M. Chhowalla, "Photoluminescence from chemically exfoliated MoS_2," Nano Lett. **11**, 5111–5116 (2011).
23. Y.-C. Lin, W. Zhang, J.-K. Huang, K.-K. Liu, Y.-H. Lee, C.-T. Liang, C.-W. Chu, and L.-J. Li, "Wafer-scale MoS_2 thin layers prepared by MoO_3 sulfurization," Nanoscale **4**, 6637–6641 (2012).
24. B. Radisavljevic, A. Radenovic, J. Brivio, V. Giacometti, and A. Kis, "Single-layer MoS_2 transistors," Nat. Nanotechnol. **6**, 147–150 (2011).
25. K. S. Novoselov, D. Jiang, F. Schedin, T. J. Booth, V. V. Khotkevich, S. V. Morozov, and A. K. Geim, "Two-dimensional atomic crystals," Proc. Natl. Acad. Sci. USA **102**, 10451–10453 (2005).
26. K. Kaasbjerg, K. S. Thygesen, and K. W. Jacobsen, "Phonon-limited mobility in n-type single-layer MoS_2 from first principles," Phys. Rev. B **85**, 115317 (2012).
27. W. Kim, A. Javey, O. Vermesh, Q. Wang, Y. Li, and H. Dai, "Hysteresis caused by water molecules in carbon nanotube field-effect transistors," Nano Lett. **3**, 193–198 (2003).
28. S. Ghatak and A. Ghosh, "Observation of trap-assisted space charge limited conductivity in short channel MoS_2 transistor," Appl. Phys. Lett. **103**, 122103 (2013).
29. A. Sourav, Z. Li, Z. Huang, V. D. Botcha, C. Hu, J.-P. Ao, Y. Peng, H.-C. Kuo, J. Wu, X. Liu, and K.-W. Ang, "Large scale transparent molybdenum disulfide plasmonic photodetector using split bull eye structure," Adv. Opt. Mater. **6**, 1800461 (2018).
30. A. E. Yore, K. K. H. Smithe, S. Jha, K. Ray, E. Pop, and A. K. M. Newaz, "Large array fabrication of high performance monolayer MoS_2 photodetectors," Appl. Phys. Lett. **111**, 043110 (2017).
31. X. Liu, H. Gu, K. Li, L. Guo, D. Zhu, Y. Lu, J. Wang, H.-C. Kuo, Z. Liu, W. Liu, L. Chen, J. Fang, K.-W. Ang, K. Xu, and J.-P. Ao, "AlGaN/GaN high electron mobility transistors with a low sub-threshold swing on free-standing GaN wafer," AIP Adv. **7**, 095305 (2017).
32. X. Liu, H. Gu, K. Li, J. Wang, L. Wang, H.-C. Kuo, W. Liu, L. Chen, J. Fang, M. Liu, X. Lin, K. Xu, and J.-P. Ao, "GaN Schottky barrier diodes on free-standing GaN wafer," ECS J. Solid State Sci. Technol. **6**, N216–N220 (2017).
33. X. Liu, J. He, Q. Liu, D. Tang, F. Jia, J. Wen, Y. Lu, W. Yu, D. Zhu, W. Liu, P. Cao, S. Han, J. Pan, Z. He, and K.-W. Ang, "Band alignment of HfO_2/multilayer MoS_2 interface determined by x-ray photoelectron spectroscopy: effect of CHF_3 treatment," Appl. Phys. Lett. **107**, 101601 (2015).
34. J. Kong, K. T. Park, A. C. Miller, and K. Klier, "Molybdenum disulfide single crystal (0002) plane XPS spectra," Surf. Sci. Spectra. **7**, 69–74 (2000).
35. D. Ruzmetov, K. Zhang, G. Stan, B. Kalanyan, G. R. Bhimanapati, S. M. Eichfeld, R. A. Burke, P. B. Shah, T. P. O'Regan, F. J. Crowne, A. G. Birdwell, J. A. Robinson, A. V. Davydov, and T. G. Ivanov, "Vertical 2D/3D semiconductor heterostructures based on epitaxial molybdenum disulfide and gallium nitride," ACS Nano **10**, 3580–3588 (2016).
36. H. Gu, Y. Lu, D. Zhu, K. Li, S. Zheng, J. Wang, K.-W. Ang, K. Xu, and X. Liu, "High temperature study on the thermal properties of few-layer $Mo_{0.5}W_{0.5}S_2$ and effects of capping layers," Results Phys. **7**, 4394–4397 (2017).
37. W. Choi, M. Y. Cho, A. Konar, J. H. Lee, G.-B. Cha, S. C. Hong, S. Kim, J. Kim, D. Jena, and J. Joo, "High-detectivity multilayer MoS_2 phototransistors with spectral response from ultraviolet to infrared," Adv. Mater. **24**, 5832–5836 (2012).
38. L. Huang, W. C. Tan, L. Wang, B. Dong, C. Lee, and K.-W. Ang, "Infrared black phosphorus phototransistor with tunable responsivity and low noise equivalent power," ACS Appl. Mater. Interfaces **9**, 36130–36136 (2017).
39. F. Xia, T. Mueller, Y.-M. Lin, A. Valdes-Garcia, and P. Avouris, "Ultrafast graphene photodetector," Nat. Nanotechnol. **4**, 839–843 (2009).
40. F. Xia, T. Mueller, R. Golizadeh-Mojarad, M. Freitag, Y.-M. Lin, J. Tsang, V. Perebeinos, and P. Avouris, "Photocurrent imaging and efficient photon detection in a graphene transistor," Nano Lett. **9**, 1039–1044 (2009).
41. G. Konstantatos, M. Badioli, L. Gaudreau, J. Osmond, M. Bernechea, F. P. G. de Arquer, F. Gatti, and F. H. L. Koppens, "Hybrid graphene-quantum dot phototransistors with ultrahigh gain," Nat. Nanotechnol. **7**, 363–368 (2012).
42. K. Nagashio, T. Yamashita, T. Nishimura, K. Kita, and A. Toriumi, "Electrical transport properties of graphene on SiO_2 with specific surface structures," J. Appl. Phys. **110**, 024513 (2011).
43. D. J. Late, B. Liu, H. S. S. R. Matte, V. P. Dravid, and C. N. R. Rao, "Hysteresis in single-layer MoS_2 field effect transistors," ACS Nano **6**, 5635–5641 (2012).